ACS APPLIED MATERIALS & INTERFACES

Letter

www.acsami.org

Self-Assembled Nanoparticles Based on Amphiphilic Anticancer Drug−Phospholipid Complex for Targeted Drug Delivery and Intracellular Dual-Controlled Release

Yang Li,[†,‡,§] Jinyan Lin,[†,‡,§] Xiangrui Yang,[‡] Yanxiu Li,[‡] Shichao Wu,[‡] Yu Huang,[‡] Shefang Ye,[‡] Liya Xie,[⊥] Lizong Dai,[*,‡] and Zhenqing Hou[*,‡]

[‡]College of Materials, and [§]Department of Chemistry, College of Chemistry and Chemical Engineering, Xiamen University, Xiamen 361005, China

[⊥]The First Affiliated Hospital of Xiamen University, Xiamen 361002, China

Supporting Information

ABSTRACT: Integrating advantages of mitomycin C (MMC)−phospholipid complex for increased drug encapsulation efficiency and reduced premature drug release, DSPE-PEG-folate (DSPE-PEG-FA) for specific tumor targeting, we reported a simple one-pot self-assembly route to prepare the MMC−phospholipid complex-loaded DSPE-PEG-based nanoparticles (MP-PEG-FA NPs). Both confocal imaging and flow cytometry demonstrated that MMC was distributed into nuclei after cellular uptake and intracellular drug delivery. More importantly, the systemically administered MP-PEG-FA NPs led to increased blood persistence and enhanced tumor accumulation in HeLa tumor-bearing nude mice. This study introduces a simple and effective strategy to design the anticancer drug−phospholipid complex-based targeted drug delivery system for sustained/controlled drug release.

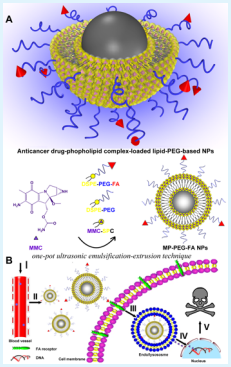

KEYWORDS: *anticancer-phospholipid complex, self-assembly, nanoparticles, targeted drug delivery, sustained/controlled drug release*

Existing chemotherapy is considered as one of the primary options to treat cancer, which is still one of the most prevalent and lethal diseases in global healthcare.[1] Mitomycin C (MMC), an effective water-soluble chemotherapy agent, has been widely used for the treatment of various cancers.[2] In addition, MMC is a poor substrate for P-glycoprotein and retains activity against many types of P-glycoprotein-mediated multidrug resistant cancer cells.[3−5] Unfortunately, the progress toward therapeutic application of MMC is greatly limited by its numerous defects, including the poor aqueous stability, nonspecific biodistribution, rapid plasma elimination, severe systemic toxicity, and narrow therapeutic window.[5]

Nanoparticles (NPs) are explosively increasing in importance as vehicles for chemotherapy agent because of their ability to enhance drug delivery efficacy and reduce drug side effects.[6] The loading of some chemotherapy agents within the NPs would be a possible approach to overcome these limitations above.[6] However, the encapsulation of water-soluble MMC drug is a great challenge for the NPs by the common preparation methods. Moreover, the water-soluble MMC drug without efficient liposolubility and lipophilicity may result in the failure of the formation of the MMC drug delivery systems.

To date, several strategies such as prodrug design,[5] phospolipid complex technique,[7] and ionic complex technique[8] have been investigated to increase the liposolubility and lipophilicity of the water-soluble MMC drug. Among these strategies, the drug-phospholipid complex technique attracted the attention of researchers to novel drug formulation more than ever, and showed the great superiority to improve the drug safety, bioavailability, and efficacy while retaining the pharmacological action of the drug.[9] Besides, phospholipid is of highly hydrophobic and superolephilic characteristics which make it an attractive choice as core architecture of drug delivery systems. Thus, the introduction of the drug-phospholipid complex into conventional drug delivery systems such as lipid or polymer-based NPs might offer a novel drug delivery approach.[9−11] In our lab, the MMC-soybean phosphatidylcholine complex (MMC-SPC) has been prepared for the development of MMC drug delivery.[7] On the one hand, MMC interacted with soybean phosphatidylcholine (SP) to form MMC-SPC via electrostatic interaction, hydrogen bonds, and van der Waals forces, and resulted in almost 100% complexation efficiency.[7] On the other hand, MMC-SPC is a reverse amphiphilic structure with water-soluble MMC molecule bounded by the hydrophilic head groups of SP molecule whereas the hydrophobic tail groups of SP molecule wrap over the complex, entrapping drug within phospholipid and resembling phospholipid in being substantially lipophilic and hydrophilic.[12]

Received: June 8, 2015
Accepted: August 3, 2015
Published: August 3, 2015

DOI: 10.1021/acsami.5b05038
ACS Appl. Mater. Interfaces 2015, 7, 17573−17581

We previously fabricated the phytosomes loaded with MMC-SPC, but the serious burst drug release consequentially limited the drug delivery efficiency of therapeutic MMC systems.[7] We also previously developed the PLA-lipid-PEG NPs loaded with MMC-SPC, but the complicated fabrication process inevitably limited the industrial-scale preparation of therapeutic MMC systems.[12,13] However, the introduction of drug-phospholipid complex into simple and robust NPs with a highly flexible and reasonable combination feature of targeted drug delivery and intracellular responsive drug release is urgently needed to be considered to greatly facilitate scaled production and clinical development.

1,2-Distearoyl-*sn*-glycero-3-phosphoethanolamine-N-[methoxy (polyethylene glycol)-2000] (DSPE-PEG), one widely used kind of phosphoethanolamine-polyethylene glycol (PE-PEG, also a commercially available phospholipid with a PEG spacer), is an attractive amphiphilic lipid-polymer conjugate including hydrophilic PEG and extremely hydrophobic fatty acids, and has been certified by FDA for clinical application. In addition, DSPE-PEG, a PEG-lipid conjugate, is not only used as a key material to form the self-assemblies widely used for anticancer drug delivery, but also utilized as an additive material to surface functionalized a variety of drug delivery systems composed of lipids, polymers, inorganic materials, and even hybrid combinations of those materials leading to the improvement of the in vitro and in vivo stability and pharmacokinetics[14−16] as a result of PEGylation-induced reduction in immunogenicity.[15,17]

Herein, based on the "from outer to inner" structural design concept, a kind of multifunctional NPs was simply fabricated for tumor-targeted intracellular drug release by synergistically integrating functions of FA for active tumor targeting, PEG for prolonged blood circulation, DSPE for efficient drug loading, MMC-SPC for pH-controlled drug release (as illustrated in Figure 1A). In this study, we used MMC-SPC, DSPE-PEG, and DSPE-PEG-FA to prepare the MP-PEG-FA NP via "one-pot ultrasonic emulsification" followed by the extrusion technique. The MP-PEG-FA NPs for in vivo tumor-targeted nuclear drug delivery should have low interactions with the blood components including blood protein and red blood cells (RBCs) to ensure a long blood circulation time, be able to passively accumulate at the tumor site and actively enter the tumor cell once in the tumor, rapidly and specifically release drug in an acidic endo/lysosomes, and deliver drug to the nucleus (Figure 1B). To our best knowledge, this is the first report that the drug-phospholipid complex (or hydrophilic drug-phospholipid complex) is introduced into the PEGylated lipid-based drug delivery systems to increase the drug loading capacity and improve drug delivery efficacy for cancer treatment.

In this paper, to further improve the selective targetability of the anticancer drug−phospholipid complex-loaded lipid-PEG-based NPs, we conjugated FA to the amine end group of DSPE-PEG-NH_2 using DCC and NHS via a DCC-mediated coupling to produce the target DSPE-PEG-FA (Figure S1), and the new amide bond was formed due to the nucleophilic reaction in the presence of triethyl amine. The ^{1}H NMR spectrum of DSPE-PEG-FA was shown in Figure 2A (^{1}H NMR spectra of DSPE-PEG-NH_2, FA, and DSPE-PEG-FA are shown in Figure S2 in the Supporting Information). The characteristic peaks of the forming amide linkage between DSPE-PEG-NH_2 and FA were detected at 8.1 ppm. In addition, DSPE-PEG-FA had the sharp proton peak of repeated units of PEG at 3.5 ppm,

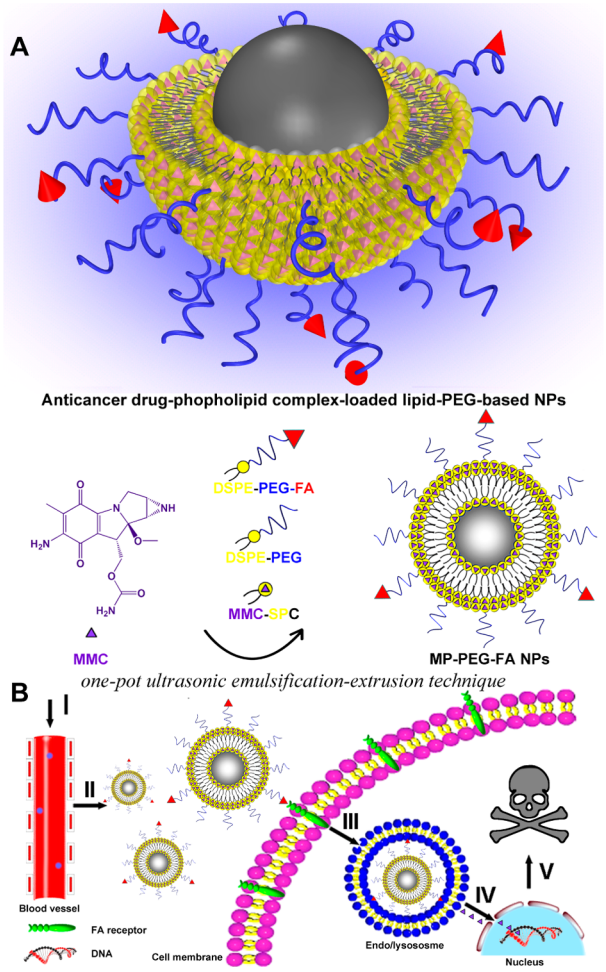

Figure 1. Schematic illustration of the preparation of the anticancer drug−phospholipid complex-loaded lipid-PEG-based NPs (MP-PEG-FA NPs), tumor-targeted accumulation, receptor-mediated endocytosis, and intracellular dual-controlled drug release. (A) Preparation and main components of MP-PEG-FA NPs, consisting of MMC-SPC (drug-phospholipid complex), DSPE-PEG (lipid-PEG conjugate), and DSPE-PEG-FA (lipid-PEG conjugate with targeting moiety). (B) Site-specific MMC drug delivery by the MP-PEG-FA NPs to nuclei for cancer treatment: (I) intravenous administration of the MP-PEG-FA NPs; (II) accumulation of the MP-PEG-FA NPs at the tumor site through passive targeting achieved by the advantage of the EPR effect; (III) FA receptor-mediated endocytosis of the MP-PEG-FA NPs by the tumor cells; (III) acid-promoted and drug-phophoslipid complex-controlled MMC release in endo/lysosomes; (IV) diffusion and accumulation of released MMC in nucleus; (V) induction of DNA damage-mediated cell apoptosis/death.

obvious proton peaks of methyl and methylene group of DSPE at 0.8 and 1.2 ppm, and characteristic proton peaks of pteridine ring and p-phenyl ring at 6.6, 7.7, and 8.6 ppm. The UV−vis spectrum of DSPE-PEG-FA was shown in Figure 2B, a sharp absorption peak at 283 was observed derived from the structure of FA. According to ATR-FITR (Figure S3 in the Supporting Information), the two characteristic peaks of DSPE-PEG-FA at 1647 and 1541 cm^{-1} was respectively ascribed to ν(NC═O) (amide I) and δ(CN-H) (amide II) vibrations, indicating the formation of an amide bond between DSPE-PEG-NH_2 and FA.[18] The strong peak exhibited at 1606 cm^{-1} was assigned to the typical N−H bending vibrations of primary amine of FA. The peaks observed at 1570, 1559, 1508, and 1457 cm^{-1} were due to aromatic skeletal vibration of benzene ring of FA. In

DOI: 10.1021/acsami.5b05038
ACS Appl. Mater. Interfaces 2015, 7, 17573−17581

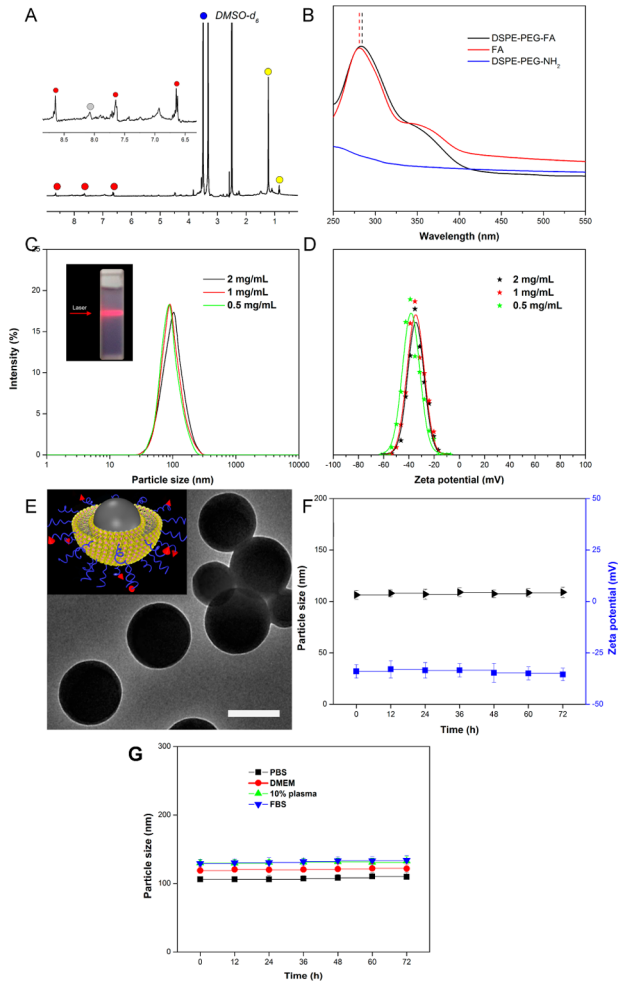

Figure 2. (A) ^{1}H NMR spectrum of DSPE-PEG-FA. (B) UV−vis spectrum of DSPE-PEG-FA. (C) Particle size and particle size distribution of the MP-PEG-FA NPs. (D) Zeta potential of the MP-PEG-FA NPs. (E) TEM image of the MP-PEG-FA NPs. Scale bar = 50 nm. (F) In vitro particle size and zeta potential stability of the MP-PEG-FA NPs in H_2O at 37 °C. (G) In vitro particle size stability of the MP-PEG-FA NPs in PBS, DEME, 10% plasma, and FBS at 37 °C. Data are presented as mean ± s.d. (n = 3).

addition, matrix-assisted laser desorption ionization time-of-flight mass spectrometry (MALDI-TOF-MS) characterization also confirmed the conjugation of FA to DSPE-PEG-NH_2 (Figure S4). All these ^{1}H NMR, UV−vis, FTIR, and MALDI-TOF-MS results suggested that FA was successfully coupled with DSPE-PEG-NH_2.

Owing to the poor physiochemical and physiological stability of MMC, we previously used mitomycin C (MMC) and SP to prepare the anticancer drug−phospholipid complex (MMC-SPC) to improve the stability and therapeutic efficacy of MMC. On the other hand, FA receptors are overexpressed on epithelial tumors of various organs, such as brain, kidney, breast, and lung, but rarely expressed in normal tissues,[19] and FA has been widely and frequently used as ligand to target the tumor cells overexpressing FA receptors. Thus, in this paper, the self-assembled nanoscaled systems for targeted drug delivery and intracellular dual-controlled release were synthesized from anticancer drug−phospholipid complex, and lipid-polymer conjugate, lipid-polymer conjugate with targeting moiety through the strong sonication method followed by the extrusion technique. MMC-SPC, DSPE-PEG, and DSPE-PEG-FA via a self-assembly process formed a hydrophobic SP/DSPE lipid core−hydrophilic PEG shell structure with FA molecules, and MMC molecules were loaded within the MP-PEG-FA NPs. Particularity, SP and DSPE served as drug delivery vehicle, PEG acted as a long-circulating agent, FA served as a targeting ligand, and MMC was used as an anticancer drug for cancer treatment.

The hydrodynamic particle size, particle size distribution, polydispersity index (PDI), zeta potential, and morphology of the MP-PEG-FA NPs were evaluated by dynamic light scattering (DLS) and transmission electron microscopy (TEM). The MP-PEG-FA NPs presented a nanoscaled particle size with a narrow particle size distribution (Figure 2C, Table 1), a high zeta potential with a negative surface charge (Figure 2D, Table 1), and a spherical shape with core−shell structure (Figure 2E). It was reported that the drug delivery systems with a particle size between 30 and 200 nm would be suitable for intravenous drug delivery because they allow for effective extravasation into the targeted tumor due to the enhanced permeability and retention (EPR) effect, which leads to preferred tumor accumulation of the drug delivery systems at the tumor site.[20] The negative surface charge of the MP-PEG-FA NPs might be explained by the presence of the SP phospholipid and DSPE lipid on the NPs' surface since the absolute value of the negative charge from the phosphate group is larger than the positive charge from the amino group in the lipid molecule. It was also reported that the surface charge of the NPs played a critical role in their both *in vitro* and *in vivo* fate including the blood circulation time and nanostructure-cell interaction.[21] Negatively charged NPs had potential for protein resistance and prolonged circulation time compared to positively charged NPs, which always strongly interacted with red blood cell and plasma protein and thus resulted in the rapid clearance from the systemic blood circulation and the limited *in vivo* effectiveness.

The electrostatic interactions, hydrogen bonds, and van der Waals forces of MMC and SP played an important role in the formation of drug-phospholipid complex and then the introduction of the drug-phospholipid complex into the lipid-polymer hybrid drug delivery systems. In addition, because of the presence of the drug ring systems, MMC may form the hydrophobic−hydrophobic interactions to some extent with the long aliphatic carbon chains of SP. So these interactions resulted in high drug encapsulation efficiency and well acceptable drug loading content (Table 1). Thus, the MP-

Table 1. Particle Size, Polydispersity Index (PDI), Zeta Potential, Drug Encapsulation Efficiency, And Drug Loading Content of the MP-PEG NPs and MP-PEG-FA NPs Determined by DLS[a]

	particle size (nm)	PDI	zeta potential (mV)	drug encapsulation efficiency (%)	drug loading content (%)
MP-PEG NPs	102.8 ± 4.9	0.162 ± 0.017	35.2 ± 3.6	96.3 ± 0.6	9.2 ± 0.3
MP-PEG-FA NPs	106.5 ± 5.4	0.187 ± 0.012	33.8 ± 2.5	95.7 ± 0.8	9.1 ± 0.2

[a]Data are presented as mean ± s.d. (n = 3).

DOI: 10.1021/acsami.5b05038
ACS Appl. Mater. Interfaces 2015, 7, 17573−17581

PEG-FA NPs with nanoscaled particle size, narrow particle size distribution, high surface charge, high drug loading capacity, and good physiological stability (see Figure 2F, 2G, discussed below) were expected to be an effective and efficient drug delivery system for intravenous administration.

A stability assay in terms of particle size and zeta potential of the MP-PEG-FA NPs was investigated in water for 72 h at 37 °C. As shown in Figure 2F, no obvious change of the particle size and zeta potential of the MP-PEG-FA NPs in water during 72 h indicated that the MP-PEG-FA NPs had a well long-term stability. A stability assay in terms of particle size of the MP-PEG-FA NPs also was tested under different physiological media: PBS, DEME, 10% plasma, and FBS.[22] The particle size of the MP-PEG-FA NPs did not significantly change, indicating the MP-PEG-FA NPs had a great stability without the presence of precipitation and phase separation in buffer saline solution, cell culture medium, plasma, and serum. In addition to the electrostatic repulsion of the MP-PEG-FA NPs (see Figure 2G), the intrinsic antiadhesion property of phospholipid (SP) and lipid (DSPE) components,[10] and the protective effect of hydrated PEG chains[12,14] against ionic strength and protein adsorption, it should be noted that the structural longevity of the MP-PEG-FA NPs by introducing the homogeneous and amorphous MMC-SPC[7] (see Figure S5−S8 in the Supporting Information) could circumvent the stability problems including encountered in the conventional liposomes. The result revealed that the MP-PEG-FA NPs could offer the protection of drugs from untimely structure disintegration and premature drug release until arriving a disease site.

The *in vitro* release profiles of the MP-PEG-FA NPs were obtained by representing the percentage of the released amount of MMC with respect to the encapsulated amount of MMC. The MP-PEG-FA NPs displayed a biphasic release behavior over 36 h similar to the MP-PEG NPs (Figure 3A), indicating that the presence of FA on the NPs' surface did not significantly alter the MMC drug release. The initial burst MMC release might be related to the presence of a part of drug-phospholipid complex absorbed on the surface of the NPs, which could be helpful to inhibit the tumor cell growth in a short time. The later sustained MMC release was attributed to the presence of drug-phospholipid complex loaded within the NPs, which could offer the possibility of continually fighting against the tumor cell. The MMC-SPC first suffered dissociation, and then the pharmaceutically active MMC diffused from the NPs, and this diffusion-controlled mechanism could reduce the nonspecific drug release by an increase of drug lipophilicity, lipophicity, and stability.

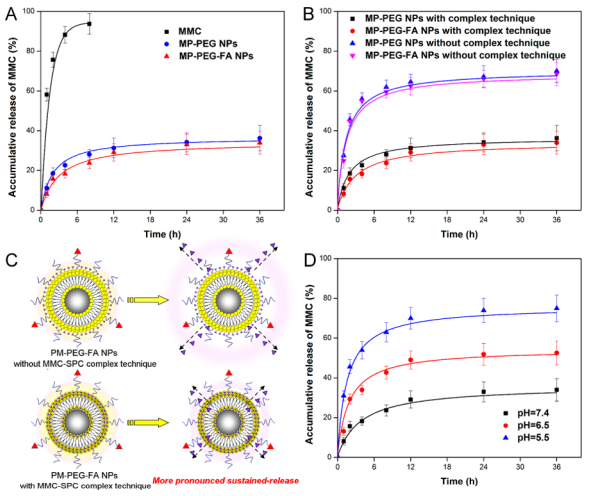

Figure 3. In vitro MMC release profile of the MP-PEG-FA NPs. (A) Time-dependent drug release of the free MMC, MP-PEG NPs, and MP-PEG-FA NPs in PBS at pH 7.4. (B) Time-dependent drug release of the MP-PEG-FA NPs with and without MMC-SPC drug-phospholipid complex technique in PBS at pH 7.4. (C) Schematic illustration of MMC release from the MP-PEG-FA NPs with and without MMC-SPC drug-phospholipid complex technique. (D) Time-dependent drug release of the MP-PEG-FA NPs in PBS at pH 5.5, 6.5, and 7.4. Data are presented as mean ± s.d. (n = 3).

It should be noted that a significant improvement on the drug encapsulation efficiency of the MP-PEG-FA NPs with complex technique (95.7 ± 0.8%) compared to the MP-PEG-FA NPs without complex technique (38.8 ± 0.6%) was most likely due to the molecular formation of drug-phospholipid complex and then the structural introduction of the drug-phospholipid complex into the lipid-polymer hybrid NPs. We hypothesized the phospholipid-MMC complex might prevent the outward diffusion of MMC during the preparation of the lipid-PEG-based NPs, which resulted in the reduced drug loss. To test the hypothesis, we performed the *in vitro* release profiles of the MP-PEG-FA NPs with complex technique and MP-PEG-FA NPs without complex technique (Figure 3B, 3C). The result indicated a delayed MMC release of the MP-PEG-FA NPs with complex technique compared with the MP-PEG-FA NPs without complex technique. The hydrophobic interactions (between DSPE lipid and SP phospholipid) and electrostatic interaction, hydrogen bonds, and van der Waals forces (between SP phospholipid and MMC drug) endowed the MP-PEG-FA NPs with the advantage of reasonable structure and strong integrity. In turn, the MMC-SPC acted as a structural element of the nanoscaled MMC drug delivery systems and served as an effective physical barrier against both MMC drug diffusion outward and water penetration inward, which resulted in decreased burst release and increased sustained release of MMC. Well-consistent with Hou's research,[13] the MMC-SPC loaded within lipid-PEG-based nanoscaled drug delivery systems, linking both the conventional and novel drug formulation, not only improved the MMC lipophilicity to increase drug encapsulation efficacy, but also controlled the MMC release to reduce systemic side effect.

The drug release from the MP-PEG-FA NPs was also evaluated in PBS at different pH values (Figure 3D). The result indicated that the drug release rate was significantly dependent on the pH value of PBS buffer. In the acidic environment (pH 5.5), the MP-PEG-FA NPs released 75.0% of MMC in 36 h. Whereas, in the neutral environment (pH 7.4), only 33.9% of MMC was released from the MP-PEG-FA NPs. The pH-triggered drug release behavior of the MP-PEG-FA NPs was related to the isoelectric points (pI) of MMC and phospholipid/lipid-PEG.[16] As the pH was adjusted from 7.4 via 6.5 to 5.5, the electrostatic repulsion force between positively charged MMC molecules (pI = 10.9)[23] was increased to promote the MMC dissociation. In addition, the negatively charged DSPE-PEG molecules (pI = 5.9)[16] and SP molecules (pI = 6.7)[24] were reversed to be positively charged and lost their electrostatic attraction force to the positively charged MMC. All results indicated the dual-controlled (pH-triggered and drug-phospholipid controlled) and sustained drug release allowed for the rapid release of MMC in slightly acidic tumor extracellular matrix (pH ≈ 6.5) and significantly acidic

DOI: 10.1021/acsami.5b05038
ACS Appl. Mater. Interfaces 2015, 7, 17573−17581

intracellular endo/lysosomes (pH = 5.0−5.5) whereas the reduced premature release of MMC during blood circulation (pH ≈ 7.4).[21]

To qualitatively investigate the cellular uptake of the MP-PEG-FA NPs, HeLa cells were incubated with the MP-PEG-FA NPs^{DiI} or MP-PEG NPs^{DiI} (DiI was encapsulated in the MP-PEG-FA NPs or MP-PEG NPs) at the equivalent DiI concentration for 6 h. The MP-PEG NPs^{DiI} showed some fluorescence signals in HeLa cells (Figure 4A, 5A). On the other hand, the MP-PEG-FA NPs^{DiI} exhibited greater fluorescence signals in HeLa cells (Figure 4A, 5A). The result indicated that the MP-PEG-FA NPs were taken up better by HeLa cells overexpressing FA receptors compared to the MP-PEG NPs, which confirmed the presence of functional FA molecules on the surface of the nanoscaled drug delivery systems. In addition, the weaker fluorescent signals were detected when HeLa cells were treated with an excess of the free FA prior to the incubation with the MP-PEG-FA NPs^{DiI}. It was suggested that the FA functionalized MP-PEG NPs specifically and selectively bound to FA receptors and were internalized by HeLa cells via FA receptors-mediated endocytosis pathway.

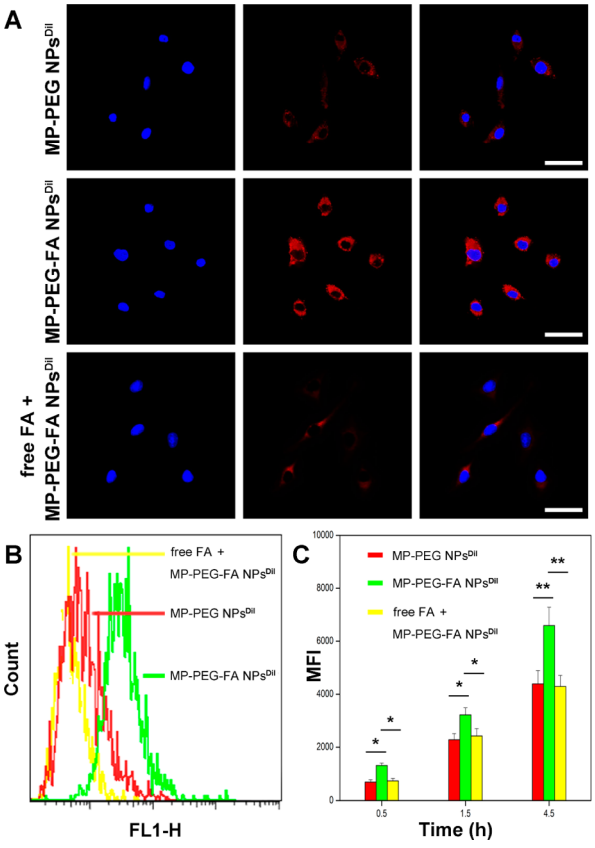

Figure 4. In vitro cellular uptake of the MP-PEG-FA NPs. (A) Confocal laser scanning microscopy images of HeLa cells incubated with the MP-PEG NPs^{DiI}, MP-PEG-FA NPs^{DiI}, and MP-PEG-FA NPs^{DiI} under the free FA blocking for 6 h. The nuclei were stained with DAPI. Red: DiI. Blue: nuclei. All the concentration of DiI was equivalent. All the scale bars represented 25 μm. All the images were taken under identical instrumental conditions. (B) Flow cytometry histogram profiles of HeLa cells incubated with the MP-PEG NPs^{DiI}, MP-PEG-FA NPs^{DiI}, and MP-PEG-FA NPs^{DiI} under the free FA blocking for 6 h. All the concentration of DiI was equivalent. (C) Flow cytometer tests of HeLa cells incubated with the MP-PEG NPs^{DiI}, MP-PEG-FA NPs^{DiI}, and MP-PEG-FA NPs^{DiI} under the free FA blocking for 0.5, 1.5, and 4.5 h. All the concentration of DiI was equivalent. Data are presented as mean ± s.d. (n = 3). * P < 0.05. ** P < 0.01 (two-tailed Student's t test).

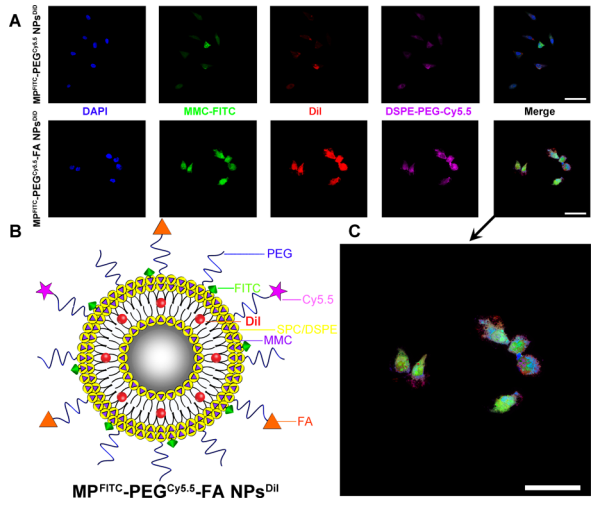

Figure 5. Intracellular drug delivery of the MP-PEG-FA NPs. (A) Confocal laser scanning microscopy images of HeLa cells incubated with the MP^{FITC}-PEG$^{Cy5.5}$ NPs^{DiI} or MP^{FITC}-PEG$^{Cy5.5}$-FA NPs^{DiI}. All the scale bars represented 25 μm. All the images were taken under identical instrumental conditions. (B) Schematic of addition of FITC, Cy5.5, and DiI for fluorescent tracking of the MP-PEG-FA NPs. The purplish red fluorescence resulted from the Cy5.5 staining served to label the lipid-PEG of the MP-PEG-FA NPs. The red fluorescence resulted from the DiI staining served to label the phospholipid/lipid of the MP-PEG-FA NPs. The green fluorescence resulted from the FITC staining served to label the MMC drug, and the blue fluorescence resulted from the DAPI staining served to label the nuclei. (C) Enlarged confocal laser scanning microscopy images of HeLa cells incubated with the MP^{FITC}-PEG$^{Cy5.5}$-FA NPs^{DiI}.

To quantitatively investigate the cellular uptake of the MP-PEG-FA NPs^{DiI}, HeLa cells were incubated with the MP-PEG-FA NPs^{DiI} for different time periods. The results (Figure 4B, 4C) further indicated the significantly increased time-dependent cellular internalization efficacy of the MP-PEG-FA NPs^{DiI} over the MP-PEG NPs^{DiI}. On the one hand, the nanoscaled particle size of the MP-PEG NPs^{DiI} and the lipophilicity of lipid on their surface via the adsorption endocytosis perhaps facilitated the transport across cell membrane and increased the cellular uptake due to the similar component between DSPE/SP of MP-PEG NPs and membrane phospholipid of HeLa cells.[13,25] On the other hand, the FA receptor-mediated endocytosis via the selective ligand−receptor interaction could further promote the cellular internalization. Utilizing both confocal scanning and flow cytometry, these qualitative and quantitative results gave a proof of the improved cellular uptake efficiency of the MP-PEG-FA NPs.

An understanding of the intracellular delivery and cellular distribution of the nanoscaled drug delivery systems is essential to achieving selective delivery of drugs at the subcellular level.[25] To further investigate the intracellular drug delivery fate of the MP-PEG-FA NPs and their intracellular drug release, we used the synthesized DSPE-PEG-Cy5.5 (Figure S9 in the Supporting Information) and MMC-FITC to be loaded within the MP-PEG-FA NPs^{DiI} (MP^{FITC}-PEG$^{Cy5.5}$-FA NPs^{DiI}) (Figure 5B). Then HeLa cells were incubated with the MP^{FITC}-PEG$^{Cy5.5}$-FA NPs^{DiI} or MP^{FITC}-PEG$^{Cy5.5}$ NPs^{DiI}, and the intracellular drug

DOI: 10.1021/acsami.5b05038
ACS Appl. Mater. Interfaces 2015, 7, 17573−17581

delivery was detected in Figure 5A,C. The blue fluorescence resulting from the DAPI staining served to label the nuclei, the green fluorescence resulted from the MMC-FITC staining served to label the anticancer drug, the red fluorescence resulted from the DiI staining served to label the phospholipid/lipid of the nanoscaled delivery vehicles, and the purplish red fluorescence resulted from the DSPE-PEG-Cy5.5 staining served to label the lipid-PEG of the nanoscaled delivery vehicles. As indicated in Figure 5, the intracellular distribution of both the nanoscaled delivery vehicles and the loaded drug was, indeed, different. A majority of the MP^{FITC}-$PEG^{Cy5.5}$-FA NPs^{DiI} was accumulated in the cytoplasm of tumor cells, possibly indicating the localization of the MP-PEG-FA NPs in the endo/lysosomes.[26] However, the drug accumulated in the cytoplasm and nucleus, which was possibly due to the fact that some drug was diffused out (released) from the MP-PEG-FA NPs, distributed through the cytoplasm, and transported inside the cells.[25] A high nuclear drug accumulation also resulted in the rapid drug diffusion to the cytoplasm.[27] In addition, HeLa cells treated with the free MMC-FITC remained with little green florescence (see Figure S10), since FITC could not be internalized by HeLa cells. Therefore, the result DiI suggest that the MP^{FITC}-$PEG^{Cy5.5}$-FA NPs^{DiI} were able to change the intracellular delivery and cellular distribution of the loaded MMC-FITC.

In a word, the drug delivered to the nuclei resulted from the efficient cellular uptake of the MP-PEG-FA NPs internalized via the FA receptor-mediated endocytosis pathway into the endo/lysosomes, and thus their effective intracellular drug release.[27] The target site of action for the MMC drug is nucleus, where the MMC drug can inhibit the DNA function and induce the tumor cell apoptosis/death. As well as the sufficient intracellular MMC drug concentration, the escape of the MMC drug delivered by the MP-PEG-FA NPs from the endo/lysosomes to nuclei was essential to exert the anticancer activity of the pharmacological and biological MMC drug.

To evaluate the cytotoxicity of the MP-PEG-FA NPs in vitro, we incubated HeLa cells with different MMC formulations in Dulbecco's modified Eagle medium (DMEM) and determined by an MTT assay (MTT = 3-(4,5-dimethylthiazol-2-yl)-2,5-diphenyltetrazolium bromide). Even though HeLa cells were not MMC-resistant, the MP-PEG NPs and MP-PEG-FA NPs showed a significantly enhanced cytotoxicity against HeLa cells compared with the free MMC (see Figure 6). Additionally, we evaluated the cytotoxicity of the MMC-free MP-PEG NPs and MP-PEG-FA NPs (P-PEG NPs and P-PEG-FA NPs). The result also showed that the delivery vehicles possessed little toxic effect to HeLa cells and DiI not affect the action mechanism of MMC. Thus, a significant increase in the cytotoxicity of the MP-PEG-FA NPs against HeLa cells compared with the MP-PEG NPs and even free MMC was attributed to the enhanced cellular internalization of the targeted NPs (see Figures 4 and 5) followed by the accelerated intracellular MMC release resulted in the increased intracellular MMC concentration (see Figurea 3 and 6).

Blood safety of nanoscaled drug delivery sytems was considered as a vital issue after intravenous administration. No apparent hemolytic effects for hemolysis analysis were observed even at the highest NP concentration of 0.8 mg/mL in 0.9% NaCl (Figure S11), which manifested that the MMC-free P-PEG NPs and P-PEG-FA NPs could not induce any hemolysis and possessed excellent blood compatibility (<2% hemolysis).

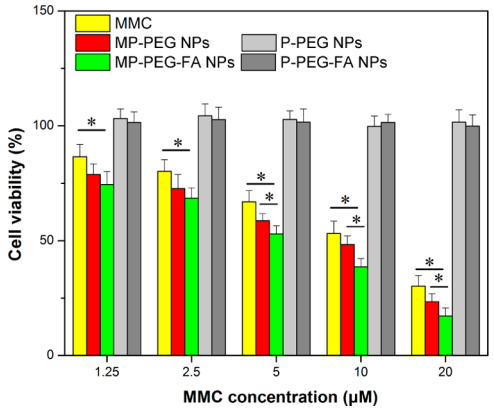

Figure 6. In vitro cell viability of the MP-PEG-FA NPs. Concentration-dependent cell viability of HeLa cells treated with the free MMC, MP-PEG NPs, MP-PEG-FA NPs, MMC-free P-PEG NPs, and MMC-free P-PEG-FA NPs after incubation of 24 h. Data are presented as mean ± s.d. (n = 6). * P < 0.05 (two-tailed Student's t test).

To investigate the in vivo pharmacokinetics of MMC, a SD rat was given a single intravenous injection of the MMC injection, MP-PEG NPs, or MP-PEG-FA NPs. After the intravenous injection, the rats treated with the MP-PEG-FA NPs and MP-PEG NPs showed initial high blood circulating levels compared with the free MMC (Figure 7). In fact, the free

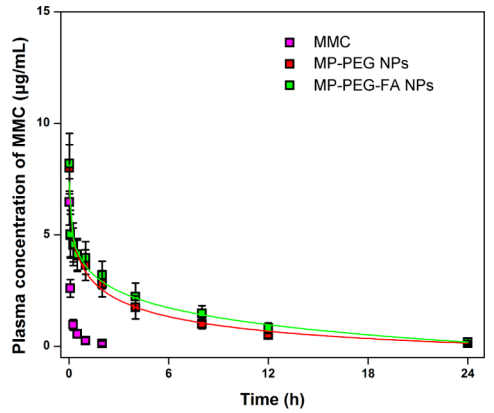

Figure 7. In vivo pharmacokinetic profile of the MP-PEG-FA NPs. Rats were intravenously injection with the free MMC, MP-PEG-FA NPs, and MP-PEG NPs. Data are presented as mean ± s.d. (n = 6).

MMC was quickly removed from the blood circulation. On the contrary, the MP-PEG-FA NPs and MP-PEG NPs exhibited a remarkably delayed blood clearance. In addition, as shown in Table 2, the MP-PEG-FA NPs and MP-PEG NPs significantly improved the pharmacokinetic parameters of MMC in comparison with the free MMC, as indicated by significantly longer elimination half-life ($t_{1/2}$), higher area under the plasma concentration versus the time curves (AUC), longer mean residence time (MRT), and lower total body clearance (CL). The result also proved the idea of the constructed lipid-PEG-based nanoscaled drug delivery systems that would prevent the rapid uptake by the reticuloendothelial system (RES), enhance the blood persistence, and prolong the blood circulation time while reducing the systemic toxicity, which had the potential to favor a combination of passive and active tumor targeting effect the MP-PEG-FA NPs.[23,28]

DOI: 10.1021/acsami.5b05038
ACS Appl. Mater. Interfaces 2015, 7, 17573−17581

Table 2. Pharmacokinetic Parameters of MMC in Rats after Intravenous Administration of MMC, MP-PEG NPs, and MP-PEG-FA NPs[a]

	MMC	MP-PEG NPs	MP-PEG-FA NPs
$t_{1/2}$ (h)	0.39 ± 0.06	4.11 ± 0.58[b]	4.63 ± 0.65[b]
AUC_{0-t} (mg h L^{-1})	1.24 ± 0.11	22.32 ± 3.72[b]	26.37 ± 4.85[b]
$AUC_{0-\infty}$ (mg h L^{-1})	1.33 ± 0.14	23.55 ± 4.67[b]	27.89 ± 3.26[b]
MRT_{0-t} (h)	0.40 ± 0.08	4.91 ± 0.75[b]	5.32 ± 0.92[b]
$MRT_{0-\infty}$ (h)	0.51 ± 0.13	5.60 ± 0.71[b]	6.31 ± 1.35[b]
CL (L h^{-1})	3.00 ± 0.14	0.15 ± 0.02[b]	0.12 ± 0.01[b]

[a]Data are presented as mean ± s.d. (n = 6). [b]$P < 0.05$ vs MMC.

To investigate the tumor-targeting ability of the MP-PEG-FA NPs, the in vivo fluorescence imaging of the HeLa tumor-bearing nude mice after the intravenous administration of the MP-PEG$^{Cy5.5}$-FA NPs was monitored using a Maestro in vivo imaging system. As shown in Figure 8, the MP-PEG$^{Cy5.5}$-FA

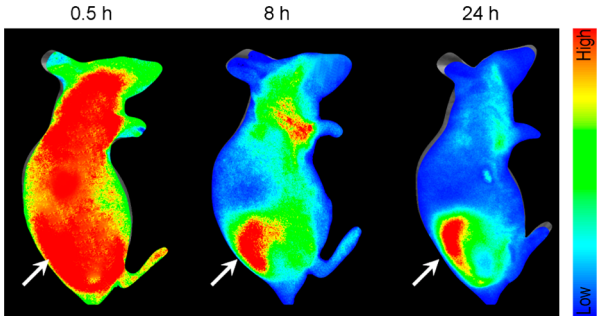

Figure 8. In vivo fluorescence imaging of the MP-PEG-FA NPs. In vivo fluorescence imaging of HeLa tumor-bearing mice after intravenous injection of the MP-PEG$^{Cy5.5}$-FA NPs at different time points postinjection. Arrows indicated the sites of tumors.

NPs were distributed in the whole body at 0.5 h postinjection. As time extended, the strong Cy5.5 fluorescence signals of the MP-PEG$^{Cy5.5}$-FA NPs were obviously detected at the tumor site at 8 h postinjection. At 24 h postinjection, the MP-PEG$^{Cy5.5}$-FA NPs exhibited the higher Cy5.5 fluorescence signals in the tumor tissue compared with in the normal tissues. In addition, the MP-PEG$^{Cy5.5}$ NPs also exhibited a similar behavior of in vivo biodistribution (Figure S12). At 24 h postinjection, the mice were sacrificed and the tumor and normal organ tissues were isolated for the ex vivo fluorescence imaging (Figure 9A). The strongest fluorescence signals were detected in the tumor tissues of mice treated with the MP-PEG$^{Cy5.5}$-FA NPs compared with other normal organ tissues, which was well-consistent with the quantitative region-of-interest (ROI) analysis (Figure 9B). It was worth noting that the stronger fluorescence signals of mice treated with the MP-PEG$^{Cy5.5}$-FA NPs were observed in the tumor tissue over the MP-PEG$^{Cy5.5}$ NPs at 24 h postinjection (Figure 9A, B). More importantly, the difference of the average fluorescence signal intensities at the tumor site between mice treated with the MP-PEG$^{Cy5.5}$-FA formulation and mice treated with the MP-PEG$^{Cy5.5}$ formulation was statistically significant ($P < 0.05$) (Figure 9B). These results suggested a superior tumor targetability of the MP-PEG$^{Cy5.5}$-FA NPs.

The accumulation of the MP-PEG$^{Cy5.5}$-FA NPs in liver tissues was due to the opsonization and uptake by the RES. The accumulation of the MP-PEG$^{Cy5.5}$ NPs in tumor tissues resulted from the passive targeting effect, which was achieved by the

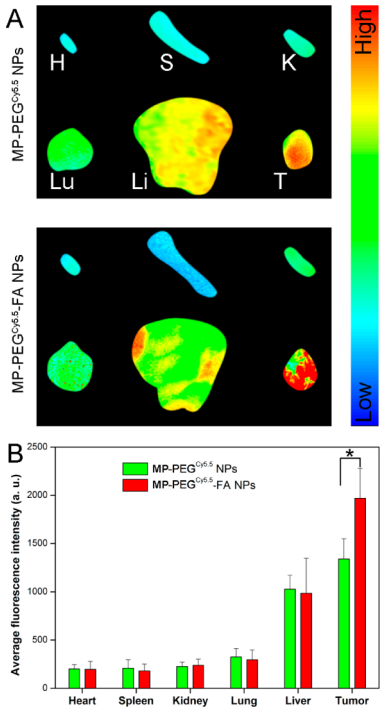

Figure 9. In vivo biodistribution of the MP-PEG-FA NPs. (A) Ex vivo fluorescence imaging of HeLa tumor-bearing mice after intravenous injection of the MP-PEG$^{Cy5.5}$ NPs and MP-PEG$^{Cy5.5}$-FA NPs at 24 h postinjection (H, heart; S, spleen; K, kidney; Lu, lung; Li, liver; T, tumor). (B) Average fluorescence signal intensities of tumors and normal tissues harvested from the HeLa tumor-bearing mice after intravenous injection of the MP-PEG$^{Cy5.5}$ NPs and MP-PEG$^{Cy5.5}$-FA NPs at 24 h postinjection. Data are presented as mean ± s.d. ($n = 3$).* $P < 0.05$ (two-tailed Student's t test).

advantage of the EPR effect due to the disorganized, leaky, and torturous tumor vasculature as well as impaired lymphatic drainage/recovery system in the tumor microenvironment.[28] Furthermore, the significantly higher tumor accumulation of the MP-PEG$^{Cy5.5}$-FA NPs compared with the MP-PEG$^{Cy5.5}$ NPs indicated that the further surface FA functionalization enhanced the tumor accumulation via not only the EPR effect-mediated passive targeting but also the FA-receptor-mediated active targeting. Collectively, it was proved that the MP-PEG-FA NPs allowed the high tumor accumulation of MMC drug mediated by a combination mechanism of passive and active targeting.

Motivated by the high tumor accumulation of the MP-PEG-FA NPs, we further investigated the in vivo anticancer efficiency by HeLa tumor-bearing nude mice. As shown in Figure 10A, the tumor growth of the mice was significantly inhibited after the treatment of different MMC formulations including the free MMC, MP-PEG NPs, and MP-PEG-FA NPs, compared with the 0.9% NaCl as a negative control. The MP-PEG NPs showed a stronger effect on inhibiting the tumor growth compared with the free MMC, which was due to the prolonged blood circulation time, passive tumor targeting effect, and controlled and sustained drug release of the nanoscaled drug delivery systems. More importantly, the MP-PEG-FA NPs exerted the strongest tumor growth inhibition effect, which was attributed to a further combination of passive (by the EPR effect) and active (by the FA receptor mediated cellular uptake) tumor targeting effect of the MP-PEG-FA NPs. In addition, the potential in vivo toxicity has always been one of great concerns in the development of nanomedicines. So, we further measured

DOI: 10.1021/acsami.5b05038
ACS Appl. Mater. Interfaces 2015, 7, 17573−17581

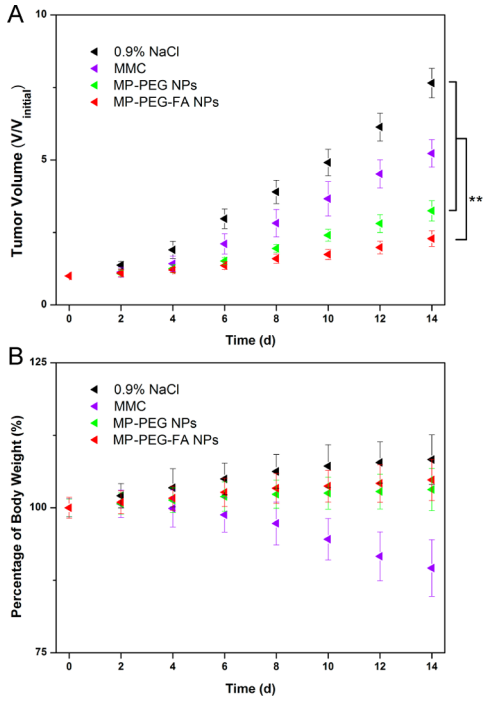

Figure 10. In vivo anticancer effect of the MP-PEG-FA NPs. (A) Tumor growth curves of HeLa tumor-bearing mice after intravenous injection of 0.9% NaCl, MMC, MP-PEG NPs, and MP-PEG-FA NPs. Data are presented as mean ± s.d. (n = 6). **P < 0.01. (two-tailed Student's t-test). (B) Body weight variations of HeLa tumor-bearing mice after intravenous injection of 0.9% NaCl, MMC, MP-PEG NPs, and MP-PEG-FA NPs. Data are presented as mean ± s.d. (n = 6).

the body weight change to evaluate the in vivo toxicity. The appreciable loss of body weight in mice was not shown found in the MP-PEG NPs and MP-PEG-FA NPs groups except for the free MMC group (Figure 10B). The result indicated a negligibly acute toxicity of the mice treated with the MP-PEG-FA NPs at the dose level specified during test time.

All results revealed that the prolonged systemic circulation time (see Figure 7, Table 2), the specific tumor accumulation and cellular uptake (see Figures 4, 5, 8, and 9), the more efficient controlled and sustained drug release (see Figure 3), and the more powerful cytotoxicity (see Figure 6) of the MP-PEG-FA NPs compared with the free MMC and MP-PEG NPs could enable the site-specific MMC drug delivery and the reinforcement on the MMC therapeutic efficacy while reducing the MMC toxicity.

3. CONCLUSIONS

In this study, by the introduction of anticancer drug−phospholipid complex into the lipid-PEG-based self-assembled drug delivery systems, the water-soluble MMC drug can be loaded within the MP-PEG-FA NPs to extend the drug retention in the blood circulation and allow the active targeting to specific tissue and dual-controllable drug release in the desirable disease site. This simple, efficient, and flexible strategy led to a promising targeted and controlled drug delivery system for cancer therapy and would assist in the further design and biomedical application of other anticancer drug−phospholipid complex-based self-assembled drug delivery systems.

■ ASSOCIATED CONTENT

Supporting Information

The Supporting Information is available free of charge on the ACS Publications website at DOI: 10.1021/acsami.5b05038.

Experimental details and additional figures (PDF)

■ AUTHOR INFORMATION

Corresponding Authors

* E-mail: houzhenqing@xmu.edu.cn. Fax: +(86)592-2183058.
*E-mail: lzdai@xmu.edu.cn.

Author Contributions

†Y.L. and J.L. contributed equally to this work.

Notes

The authors declare no competing financial interest.

■ ACKNOWLEDGMENTS

This work was funded by the National Natural Science Foundation of China (Grant 31271071), and the Fujian Province Medical Innovation Project (2014-CXB-350).

■ REFERENCES

(1) Jemal, A.; Bray, F.; Center, M. M.; Ferlay, J.; Ward, E.; Forman, D. Global Cancer Statistics. *Ca-Cancer J. Clin.* **2011**, *61*, 69−90.
(2) Schwartz, H. S.; Sodergren, J. E.; Philips, F. S.; Mitomycin, C. Chemical and Biological Studies on Alkylation. *Science* **1963**, *142*, 1181−1183.
(3) Ekins, S.; Kim, R. B.; Leake, B. F.; Dantzig, A. H.; Schuetz, E. G.; Lan, L.-B.; Yasuda, K.; Shepard, R. L.; Winter, M. a.; Schuetz, J. D.; Wikel, J. H.; Wrighton, S. A. Application of Three-Dimensional Quantitative Structure-Activity Relationships of P-Glycoprotein Inhibitors and Substrates. *Mol. Pharmacol.* **2002**, *61*, 974−981.
(4) Ekins, S.; Kim, R. B.; Leake, B. F.; Dantzig, A. H.; Schuetz, E. G.; Lan, L.-B.; Yasuda, K.; Shepard, R. L.; Winter, M. A.; Schuetz, J. D.; Wikel, J. H.; Wrighton, S. A. Three-Dimensional Quantitative Structure-Activity Relationships of Inhibitors of P-Glycoprotein. *Mol. Pharmacol.* **2002**, *61*, 964−973.
(5) Gabizon, A.; Amitay, Y.; Tzemach, D.; Gorin, J.; Shmeeda, H.; Zalipsky, S. Therapeutic Efficacy of a Lipid-Based Prodrug of Mitomycin C in Pegylated Liposomes: Studies with Human Gastro-Entero-Pancreatic Ectopic Tumor Models. *J. Controlled Release* **2012**, *160*, 245−253.
(6) Davis, M. E.; Chen, Z. G.; Shin, D. M. Nanoparticle Therapeutics: An Emerging Treatment Modality for Cancer. *Nat. Rev. Drug Discovery* **2008**, *7*, 771−782.
(7) Hou, Z.; Li, Y.; Huang, Y.; Zhou, C.; Lin, J.; Wang, Y.; Cui, F.; Zhou, S.; Jia, M.; Ye, S.; Zhang, Q. Phytosomes Loaded with Mitomycin C-Soybean Phosphatidylcholine Complex Developed for Drug Delivery. *Mol. Pharmaceutics* **2013**, *10*, 90−101.
(8) Iyengar, B. S.; Takahashi, T.; Remers, W. A.; Bradner, W. T. Metal Complexes of Mitomycins. *J. Med. Chem.* **1986**, *29*, 144−147.
(9) Khan, J.; Alexander, A.; Ajazuddin; Saraf, S.; Saraf, S. Recent Advances and Future Prospects of Phyto-Phospholipid Complexation Technique for Improving Pharmacokinetic Profile of Plant Actives. *J. Controlled Release* **2013**, *168*, 50−60.
(10) Peng, Q.; Wei, X. Q.; Shao, X. R.; Zhang, T.; Zhang, S.; Fu, N.; Cai, X. X.; Zhang, Z. R.; Lin, Y. F. Nanocomplex Based on Biocompatible Phospholipids and Albumin for Long-Circulation Applications. *ACS Appl. Mater. Interfaces* **2014**, *6*, 13730−13737.
(11) Wu, C.; Zhang, M.; Zhang, Z.; Wan, K. W.; Ahmed, W.; Phoenix, D. A.; Elhissi, A. M.; Sun, X. Thymopentin Nanoparticles Engineered with High Loading Efficiency, Improved Pharmacokinetic Properties, and Enhanced Immunostimulating Effect Using Soybean Phospholipid and Phbhhx Polymer. *Mol. Pharmaceutics* **2014**, *11*, 3371−3377.

DOI: 10.1021/acsami.5b05038
ACS Appl. Mater. Interfaces 2015, 7, 17573−17581

(12) Li, Y.; Wu, H.; Yang, X.; Jia, M.; Li, Y.; Huang, Y.; Lin, J.; Wu, S.; Hou, Z. Mitomycin C-Soybean Phosphatidylcholine Complex-Loaded Self-Assembled PEG-Lipid-Pla Hybrid Nanoparticles for Targeted Drug Delivery and Dual-Controlled Drug Release. *Mol. Pharmaceutics* **2014**, *11*, 2915−2927.
(13) Li, Y.; Lin, J.; Wu, H.; Jia, M.; Yuan, C.; Chang, Y.; Hou, Z.; Dai, L. Novel Methotrexate Prodrug-Targeted Drug Delivery System Based on PEG-Lipid-Pla Hybrid Nanoparticles for Enhanced Anticancer Efficacy and Reduced Toxicity of Mitomycin C. *J. Mater. Chem. B* **2014**, *2*, 6534−6548.
(14) Zhang, L.; Chan, J. M.; Gu, F. X.; Rhee, J. W.; Wang, A. Z.; Radovic-Moreno, A. F.; Alexis, F.; Langer, R.; Farokhzad, O. C. Self-Assembled Lipid-Polymer Hybrid Nanoparticles: A Robust Drug Delivery Platform. *ACS Nano* **2008**, *2*, 1696−1702.
(15) Sengupta, S.; Eavarone, D.; Capila, I.; Zhao, G.; Watson, N.; Kiziltepe, T.; Sasisekharan, R. Temporal Targeting of Tumour Cells and Neovasculature with a Nanoscale Delivery System. *Nature* **2005**, *436*, 568−572.
(16) Wei, T.; Liu, J.; Ma, H.; Cheng, Q.; Huang, Y.; Zhao, J.; Huo, S.; Xue, X.; Liang, Z.; Liang, X. J. Functionalized Nanoscale Micelles Improve Drug Delivery for Cancer Therapy in Vitro and in Vivo. *Nano Lett.* **2013**, *13*, 2528−2534.
(17) Allen, T. M. Ligand-Targeted Therapeutics in Anticancer Therapy. *Nat. Rev. Cancer* **2002**, *2*, 750−763.
(18) Wang, C. F.; Makila, E. M.; Kaasalainen, M. H.; Hagstrom, M. V.; Salonen, J. J.; Hirvonen, J. T.; Santos, H. A. Dual-Drug Delivery by Porous Silicon Nanoparticles for Improved Cellular Uptake, Sustained Release, and Combination Therapy. *Acta Biomater.* **2015**, *16*, 206−214.
(19) Liu, C.; Yuan, J.; Luo, X.; Chen, M.; Chen, Z.; Zhao, Y.; Li, X. Folate-Decorated and Reduction-Sensitive Micelles Assembled from Amphiphilic Polymer-Camptothecin Conjugates for Intracellular Drug Delivery. *Mol. Pharmaceutics* **2014**, *11*, 4258−4269.
(20) Allen, T. M.; Cullis, P. R. Drug Delivery Systems: Entering the Mainstream. *Science* **2004**, *303*, 1818−1822.
(21) Du, J. Z.; Sun, T. M.; Song, W. J.; Wu, J.; Wang, J. A Tumor-Acidity-Activated Charge-Conversional Nanogel as an Intelligent Vehicle for Promoted Tumoral-Cell Uptake and Drug Delivery. *Angew. Chem., Int. Ed.* **2010**, *49*, 3621−3626.
(22) Zheng, M.; Zhao, P.; Luo, Z.; Gong, P.; Zheng, C.; Zhang, P.; Yue, C.; Gao, D.; Ma, Y.; Cai, L. Robust Icg Theranostic Nanoparticles for Folate Targeted Cancer Imaging and Highly Effective Photothermal Therapy. *ACS Appl. Mater. Interfaces* **2014**, *6*, 6709−6716.
(23) Li, Y.; Lin, J.; Wu, H.; Chang, Y.; Yuan, C.; Liu, C.; Wang, S.; Hou, Z.; Dai, L. Orthogonally Functionalized Nanoscale Micelles for Active Targeted Codelivery of Methotrexate and Mitomycin C with Synergistic Anticancer Effect. *Mol. Pharmaceutics* **2015**, *12*, 769−782.
(24) Chain, E.; Kemp, I. The Isoelectric Points of Lecithin and Sphingomyelin. *Biochem. J.* **1934**, *28*, 2052−2055.
(25) Savic, R.; Luo, L.; Eisenberg, A.; Maysinger, D. Micellar Nanocontainers Distribute to Defined Cytoplasmic Organelles. *Science* **2003**, *300*, 615−618.
(26) Jin, E.; Zhang, B.; Sun, X.; Zhou, Z.; Ma, X.; Sun, Q.; Tang, J.; Shen, Y.; Van Kirk, E.; Murdoch, W. J.; Radosz, M. Acid-Active Cell-Penetrating Peptides for in Vivo Tumor-Targeted Drug Delivery. *J. Am. Chem. Soc.* **2013**, *135*, 933−940.
(27) Han, S.; Liu, Y.; Nie, X.; Xu, Q.; Jiao, F.; Li, W.; Zhao, Y.; Wu, Y.; Chen, C. Efficient Delivery of Antitumor Drug to the Nuclei of Tumor Cells by Amphiphilic Biodegradable Poly(L-Aspartic Acid-Co-Lactic Acid)/Dppe Co-Polymer Nanoparticles. *Small* **2012**, *8*, 1596−1606.
(28) Danhier, F.; Feron, O.; Preat, V. To Exploit the Tumor Microenvironment: Passive and Active Tumor Targeting of Nanocarriers for Anti-Cancer Drug Delivery. *J. Controlled Release* **2010**, *148*, 135−146.

DOI: 10.1021/acsami.5b05038
ACS Appl. Mater. Interfaces 2015, 7, 17573−17581